

Stable chaos

Antonio Politi^{1,2} and Alessandro Torcini^{1,2,3}

¹ Istituto dei Sistemi Complessi, Consiglio Nazionale delle Ricerche, via Madonna del Piano 10, I-50019 Sesto Fiorentino, Italy

² Centro Studi Dinamiche Complesse, via Sansone 1, I-50019 Sesto Fiorentino, Italy

³ Istituto Nazionale Fisica Nucleare - Sezione di Firenze, via Sansone 1, I-50019 Sesto Fiorentino, Italy

Abstract. *Stable chaos* is a generalization of the chaotic behaviour exhibited by cellular automata to continuous-variable systems and it owes its name to an underlying irregular and yet linearly stable dynamics. In this review we discuss analogies and differences with the usual deterministic chaos and introduce several tools for its characterization. Some examples of transitions from ordered behavior to stable chaos are also analyzed to further clarify the underlying dynamical properties. Finally, two models are specifically discussed: the diatomic hard-point gas chain and a network of globally coupled neurons.

1 Introduction

Chaos is associated with an exponential sensitivity of the evolution to tiny perturbations in the initial conditions, so that the presence of at least one positive Lyapunov exponent is considered as a necessary and sufficient condition for the occurrence of irregular dynamics in deterministic dynamical systems [1]. In fact, the first observation in coupled-map models of stochastic-like behaviour accompanied by a negative maximum Lyapunov exponent came as a big surprise [2,3]. In order to highlight the unexpected coexistence of *local stability* and *chaotic behaviour*, the phenomenon was called *stable chaos* (SC). Although the definition sounds like an oxymoron, in practice, there is no logical inconsistency, as the irregular behaviour is a transient phenomenon that is restricted to finite-time scales. In spite of this restriction, SC is both a well defined and meaningful concept, because the transient duration diverges exponentially with the system size and is therefore infinite in the thermodynamic limit. Moreover, the stationarity of SC [3] suggests that it can represent an interesting platform for studying non-equilibrium phenomena. A better understanding of SC can be gained by exploring the analogy with the chaotic behaviour exhibited by elementary cellular automata [4], another phenomenon that can be formally defined only in the thermodynamic limit. In fact, as we clarify in this review, SC is a sort of extension of cellular-automaton dynamics to continuous-variable systems. In particular, the spreading velocity of localized perturbations, a standard indicator used to quantify the degree of chaoticity in cellular automata, proves rather

fruitful also to characterize SC. However, in this latter case it is necessary to distinguish between finite and infinitesimal perturbations (the latter ones cannot even be defined in cellular automata, because of the discreteness of the local variable) and it is thereby possible to define two conceptually different propagation velocities. This allows giving a fairly general definition of SC as that of a dynamics dominated by “finite amplitude” perturbations [5,6].

Altogether, one can express the relevant difference between deterministic chaos and SC by referring to the relevant flux of information: while in the former context, information flows from the least towards the most significant digits, in the latter, it flows from the boundaries towards the core of the system. It would be therefore desirable to develop a general formalism able to encompass both phenomena. A promising idea is based on the introduction of “non democratic” norms which attribute increasingly small weights to the sites that are increasingly “far” from the region of interest. Although this approach allows quantifying the spatial information flow, it can be hardly extended to account for perturbations that have locally a finite amplitude, the analysis of which would require a genuine nonlinear treatment. In fact, a tool like finite amplitude Lyapunov exponents (FALEs) [7] appears to be more appropriate for characterizing SC, although it is not clear how to go beyond the maximal exponent (for the absence of a proper scalar product definition in this context).

As we have mentioned above, in systems with a finite number of degrees of freedom, SC is a transient phenomenon. One might therefore think of using tools and ideas developed for the characterization of transients such as those extensively discussed in the nice review by Tèl and Lai [8]. One must however distinguish between SC and standard chaotic transients (for a seminal paper on the subject, see [9]). In the former case, the maximum Lyapunov exponent is positive and formulas such as Kapral-Yorke and Pesin relations can be invoked to express some properties of the invariant measure in terms of the Lyapunov exponents [10]. In SC, a straightforward application of the same formulas yields manifestly useless predictions, as they do not take into account the spatial information flow that is the key mechanism of SC. Accordingly, one must still heavily rely on direct numerical simulations to infer the structure of the invariant measure. Nevertheless, we suspect that a possible common property of chaotic transients and SC is the presence of a strange repeller. In fact, chaotic transients are almost by definition the manifestation of trajectories evolving in the vicinity of a repeller, possibly characterized by a small escape rate [8,10]. This property seems to clash with the absence of unstable orbits in most of the models exhibiting SC. However, such models are also characterized by discontinuities in phase-space and here below we argue that their smoothing gives birth to a web of unstable orbits. We are thereby lead to conjecture that even though SC is accompanied by a negative Lyapunov exponent, its very existence requires the presence of topological chaos, i.e. of a finite topological entropy. When and whether the

resulting transient dynamics is linearly stable or unstable remains however to be clarified.

The review is organized in the following way. In Sec. 2 we briefly introduce the reference models that have mostly used to characterize SC. In section 3 we properly define SC from the scaling behaviour of the transient length and discuss its properties in terms of space-time correlations and fractal dimensions. Then, in Sec. 4, we discuss the relationship with cellular automata by suitably encoding the space-time pattern. In particular, we focus our attention on the indeterminacy of the next symbol as a way to quantify the difference between the original dynamics and that of a suitable deterministic automaton rule. We also introduce and estimate the propagation velocity of localized perturbations. In Sec. 5, we compare SC with the usual deterministic chaos. This is done by smoothing an otherwise discontinuous coupled-map model and studying the dependence of standard indicators such as the maximum Lyapunov exponent on the smoothness of the dynamic rule. As a result, we identify two thresholds: (i) the first one separates the regions with positive and negative Lyapunov exponent; (ii) the second, larger, threshold separates the region where finite-amplitude perturbations propagate faster than infinitesimal ones, from that where the two velocities coincide with one another (which is the signature of a standard chaotic evolution). Moreover, we compute the multifractal spectrum of the Lyapunov exponent, showing that it has a positive tail even when the average exponent itself is negative. In section 6 we discuss various order-to-chaos transitions. In fact, the analogy with cellular automata reminds us that such rules are not necessarily chaotic. The intrinsic absence of a continuous parameter makes it impossible to investigate order-to-chaos transitions in the cellular-automata context. As this restriction does not apply to SC, it makes sense and it is desirable to investigate the onset of chaotic dynamics in this latter context. We first study a coupled-map lattice, the coupling strength being the relevant control parameter. The analysis reveals the existence of a fuzzy transition region, where regular and irregular dynamics alternate in a complex manner [11]. A simple stochastic model is then introduced to gain some further insight. In the new setup, the transition is of directed-percolation type [12].

For a long time, SC has been found only in abstract mathematical models, characterized by the presence of discontinuities or nearly discontinuous ¹ evolution rules. This restriction has therefore casted some doubts on the physical relevance of this phenomenon. In Sec. 7 we discuss a mechanism that can generically lead to discontinuities in physically meaningful contexts. The mechanisms requires just the presence of δ -like events such elastic collisions between particles or spike emissions by neurons. The “non-commutativity” of such events represents a genuine source of discontinuities, which may, in turn, give rise to SC. A diatomic hard-point gas and a network of coupled neurons are discussed in Sec. 7 as examples of such dynamical systems. The

¹ See the next section for a clarification of this concept.

neural network model allows us also to discuss an order-to-chaos transition that appears to be of “standard” type (the critical region reduces to a single point), although the universality class has not yet been identified [13]. Finally the still open problems are briefly summarised in Sec. 8.

2 Models

Most of the numerical studies of *stable chaos* have been carried out in a 1D lattice of diffusively coupled maps [14],

$$x_i(t+1) = (1-\varepsilon)f(x_i(t)) + \frac{\varepsilon}{2}[f(x_{i-1}(t)) + f(x_{i+1}(t))] \quad (1)$$

where $\varepsilon \in [0 : 1]$ is the coupling constant and the map of the interval f is piecewise linear,

$$f(x) = \begin{cases} p_1x + q_1 & 0 \leq x \leq x_c \\ 1 - (1 - q_2)(x - x_c)/\eta & x_c < x < x_c + \eta \\ q_2 + p_2(x - x_c - \eta) & x_c + \eta < x \leq 1, \end{cases} \quad (2)$$

where $x_c = (1 - q_1)/p_1$. The model [5] is a continuous generalization of the systems analysed in [2] and [3], which basically correspond to $\eta = 0$, i.e. to a two-branch maps. The map is continuous because the left and right limits in the both connecting points do coincide ($f(x_c^-) = f(x_c^+)$, $f(x_c^- + \eta) = f(x_c^+ + \eta)$). Occasionally in this review we speak of “quasi-discontinuous” models, implying the presence of large but localized (in phase-space) amplifying regions. In this context, this amounts to assuming a small but non-zero width η for the middle branch. In next the section we restrict our analysis to the case $\eta = 0$.

Since this model is rather artificial (no specific physical problem lies behind the choice of f , which has been mostly selected for simplicity reasons and for coherence with the seminal paper [15]), we find it convenient to consider a second type of model, namely a chain of Duffing oscillators

$$\ddot{x}_i = -\gamma\dot{x}_i - x_i^3 + D(x_{i-1} + x_{i+1}) + (1 + G(t) \sin 2\pi t/T_1)x_i \quad (3)$$

where γ controls the dissipation, D the diffusion between nearby sites and $G(t)$ is the modulation amplitude that is periodically switched on and off; $G = A$ for $\text{mod}(t, T) < T_1$ and zero otherwise. As discussed in [4], for T_2 long enough, the Lyapunov exponent is negative, so that the evolution must eventually converge towards a periodic orbit, as it indeed does.

3 Definition and characterization of stable chaos

Simulations of the above defined map have revealed the existence of long-lasting transients followed by a sudden convergence towards some periodic

orbit. This suggests, and simulations confirm, that the basin of attraction of such orbits is so intricate that the convergence is exponential only for distances *homogeneously* smaller than some threshold θ . However, since there exist many different periodic orbits, one cannot estimate the transient length by determining the distance from an a priori unknown final state. One can nevertheless determine the distance $d(t, \tau)$ of the configuration $\{x_i(t)\}$ ($i = 1, N$) at time t from any previous configuration at time $\tau < t$. As soon as there exists a τ -value such $d(t_c, \tau) < \theta$, we can conclude that $d(t + t', \tau + t')$ will tend to 0, indicating that the dynamics converges towards an orbit of period $t - \tau$. As shown in Fig. 1, the average (over different choices of the initial conditions) transient time may increase exponentially with the chain length, i.e. with the phase space dimension. This indicates that in the thermodynamic limit, the relevant dynamical regime is not the asymptotic periodic behavior that is practically unreachable, but what one would naively consider a transient regime. This scenario is reminiscent of the disordered

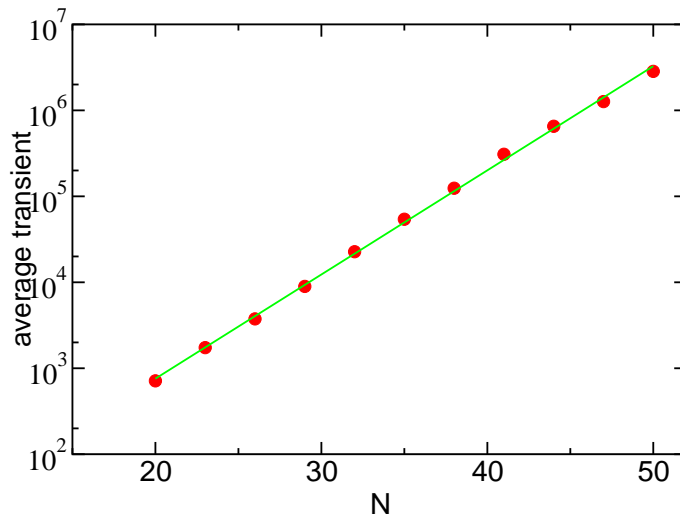


Fig. 1. Average transient duration versus the chain length for the diffusively coupled lattice of maps (2), for $p_1 = 2.7$, $q_1 = 0.$, $\eta = 0$, $q_2 = 0.07$, $p_2 = 0.1$, and for the coupling strength $\varepsilon = 2/3$.

regime in directed percolation, which, in finite systems, has necessarily a finite lifetime, as the dynamics sooner or later is absorbed by the homogeneous state [16,17]. Irrespective of this difficulty, the disordered regime is a true “phase” in the statistical-mechanics sense, as it is stable in infinite systems, i.e. when the thermodynamic limit is taken before the infinite-time limit. It should, however, be noticed that in SC the “absorbing state” is not just a

single homogenous configuration, but may be a set of different and possibly exponentially long orbits.

A second striking character of the transient is that the maximum Lyapunov exponent turns out to be negative. Like for the very existence of SC, this statement is formally correct only under the assumption of taking first the thermodynamic limit. In practice, it is sufficient that the transient duration is long enough to guarantee a good statistical convergence. From the data reported in Fig. 1, one can see that this is not a limitation at all, since already in a lattice of 100 maps, the periodic state is practically unreachable.

The very fact that the transient is Lyapunov-stable makes it substantially different from the chaotic transients that have been often found and attributed to the existence of some chaotic saddle of high dimensionality [8]. This is all the way more surprising once we notice that the “transient” dynamics is far from regular. In fact, simulations reveal that both spatial and temporal correlations decay exponentially. An example is reported in Fig. 2, where we plot

$$C(j) = \frac{|\langle x_i(t)x_{i+j}(t) \rangle|}{\langle x_i(t)^2 \rangle} \quad , \quad C(\tau) = \frac{|\langle x_i(t)x_i(t+\tau) \rangle|}{\langle x_i(t)^2 \rangle} \quad (4)$$

where $\langle \cdot \rangle$ denotes an ensemble average

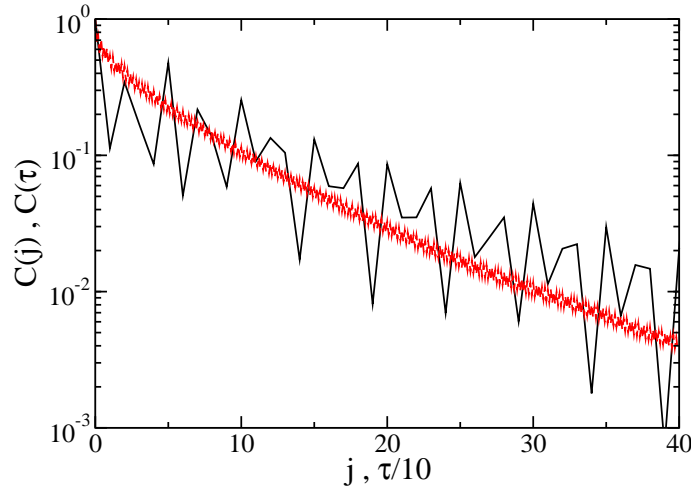


Fig. 2. Spatial and temporal (smoother curve) correlations for the same parameter values of the single map as in Fig. 1 and $\varepsilon = 0.608$.

It is natural to characterize the invariant measure also in terms of its fractal dimension. Since the whole Lyapunov spectrum is negative, one cannot

invoke the Kaplan-Yorke [18] formula to predict the number of active degrees of freedom. Actually, such a formula would imply that the dimension is equal to zero and this is in fact true for the asymptotic attractor. Therefore, we must rely only on direct numerical computations. More precisely, we have

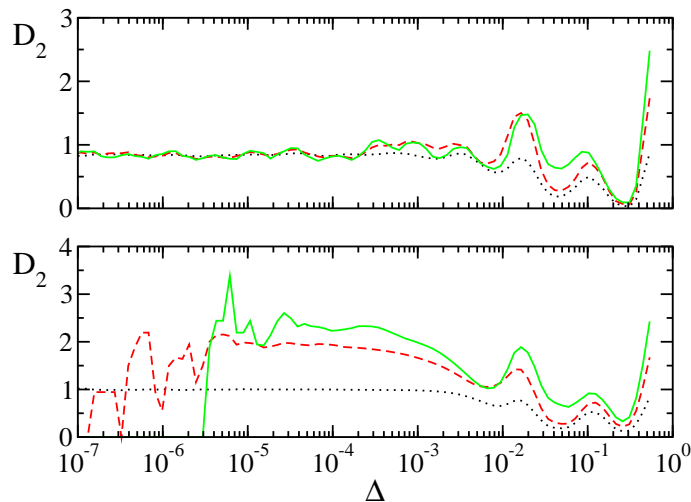


Fig. 3. Correlation dimension of the spatial embedding for $\varepsilon = 0.6008$ (upper panel) and $\varepsilon = 0.608$ (lower panel). Dotted, dashed and solid curves correspond to embedding dimension $e = 1, 2$, and 3 , respectively.

decided to compute the correlation dimension [19] of spatial sequences of variables [20]. In other words, we have constructed embedding spaces of the type $x_i(t), x_{i+1}(t), \dots, x_{i+e}(t)$, for $e = 1, 2, 3$. In each case, we have counted the number of pairs of points $\mathcal{N}(e, \delta)$ that are separated by a distance larger than Δ in a space of dimension e . Afterwards, we have determined the dimension as the effective derivative, i.e.

$$D_2(e, \Delta) = \frac{\partial \log \mathcal{N}}{\partial \log \Delta} \quad (5)$$

Formally, the correlation dimension is the limit of $D_2(e, \Delta)$ for $\Delta \rightarrow 0$. As for small Δ , \mathcal{N} is affected by statistical fluctuations due to the finite number of points, the relevant question is whether the limiting behaviour sets in for distances that are numerically accessible. In Fig. 3 we report the results for two different values of the coupling strength, $\varepsilon = 0.6008$ and $\varepsilon = 0.608$, which correspond to an ordered and chaotic regime, respectively. Even in the ordered regime, the fractal dimension is finite, as revealed by the plateau, whose height is independent of the embedding dimension. The non-zero value of the dimension reflects the disordered spatial structure, i.e. the existence of *spatial*

chaos. Therefore, already from this simple case we can conclude on the necessity to go beyond the standard Lyapunov-exponent analysis. In the chaotic regime, the effective dimension is larger and grows with the embedding dimension e (see lower panel in Fig. 3). However, in the absence of theoretical arguments, we cannot definitely conclude whether the dimension will saturate for $e \rightarrow \infty$, indicating the existence of a low-dimensional attractor, or whether it diverges, suggesting some form extensivity [20].

4 Relationship with cellular automata

The existence of a stochastic-like dynamics accompanied by an exponential contraction of infinitesimally close trajectories suggests an analogy with the so-called chaotic cellular automata (CA) rules [21]. In fact, in a finite lattice, any CA rule must eventually produce a periodic orbit, since the number of distinct states is finite, namely B^N , where B is the number of states of the local variable and N is the number of lattice sites. What makes a chaotic rule different from an ordered one is precisely the time needed to cycle through previously visited states: such a time is exponentially long in chaotic rules [21].

A binary representation of the dynamics observed in the the coupled map lattice (1) confirms these expectations. The pattern plotted in Fig. 4 are indeed very reminiscent of those obtained by iterating CA rules.

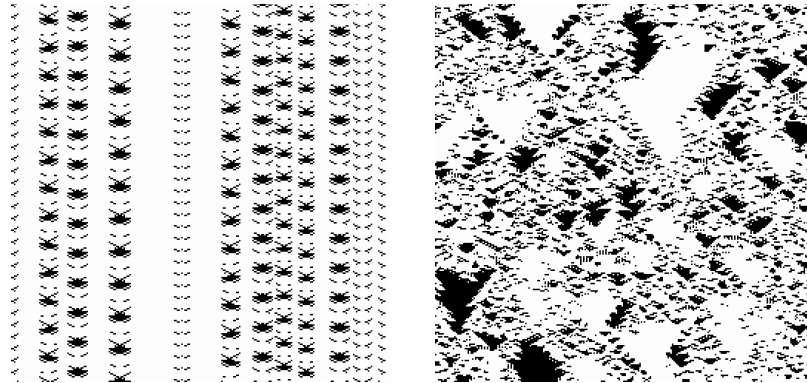


Fig. 4. Two patterns generated by iterating Eq. (1) with the function f defined as in Eq. (2) with the same parameter values as in the previous figures and coupling strength $\varepsilon = 0.55$ (left panel) and 0.7 (right panel). Time flows downwards; black corresponds to $x^i(t) < 1/2$.

The relationship with CA can be put on more firm grounds, as we discuss in the following with reference to the chain of Duffing oscillators (3).

The bistable character of the single oscillators suggests a natural way to encode the underlying dynamics and thereby to explore possible connections with CA rules. An appropriate indicator to do so is the indeterminacy $\Delta h(m)$ of the symbol $s' = s_i(t+1)$, under the assumption that the sequence $S(m) = \{s_{i-r}(t), s_{i-r+1}(t), \dots, s_i(t), \dots, s_{i+r}(t)\}$, is observed at time t (time being measured in periods of the forcing term) and where $m = 2r + 1$. The indeterminacy is formally defined as [22]

$$\Delta h(m) = \sum_S P(S(m)) \sum_{s'} P(s'|S(m)) \log P(s'|S(m)) \quad (6)$$

where the first sum extends over all sequences of length m generated by the chain dynamics, and the second sum to the two values of the symbol s' . $P(S(m))$ is the probability to observe anywhere the sequence $S(m)$; $P(s'|S(m))$ is the conditional probability that the observation of the symbol s' at time $t+1$ on the site i is preceded by the sequence S at time t in a window of length m centered around the site i . When the knowledge of $S(m)$ allows to perfectly predict s' , then the indeterminacy is zero. In this case, the symbolic dynamics is perfectly equivalent to that of a CA defined over a window of length m . In Fig. 5 we report the data for $T_2 = 8, 18$ and 20 . Δh is a non decreasing function of m , since the more we assume to know on the past, the smaller must be the uncertainty on the future. If Δh becomes exactly equal to 0 for a finite m , then we can conclude that the dynamics is perfectly reconstructible from a CA with a finite interaction range. In all cases we see that for m larger than 15, the curves saturate revealing the existence of a residual uncertainty. This does neither imply that the dynamics contains some degree of stochasticity, nor that the model has to include longer memory terms. One striking such example was discussed in Ref. [22], where Crutchfield applied this approach to the pattern generated by an elementary CA, after it was suitably encoded. The indeterminacy of the encoded pattern revealed the presence of a residual uncertainty even though the CA rule is deterministic and requires only the memory of one past step, while the encoding is even memoryless. The identification of the “optimal machine” in generic cases is a typical example of the hardness of inverse problems.

The analogy with CA suggests to quantify the degree of chaos also in SC by determining the velocity v_F of propagation of perturbations. Let us consider two configurations that initially differ in the interval $[-r, r]$ and let $i_l(t)$ ($i_r(t)$) denote the leftmost (rightmost) site where they differ more than some threshold. Accordingly, we can define the front velocity as

$$v_F = \lim_{t \rightarrow \infty} \frac{i_r - i_l}{2t}. \quad (7)$$

Within CAs, a finite spreading velocity is considered as an evidence of chaotic behaviour [21]. In fact, this is true also in the context of SC, as it can be seen in Fig. 6, where we plot the spreading of an initial difference for parameter

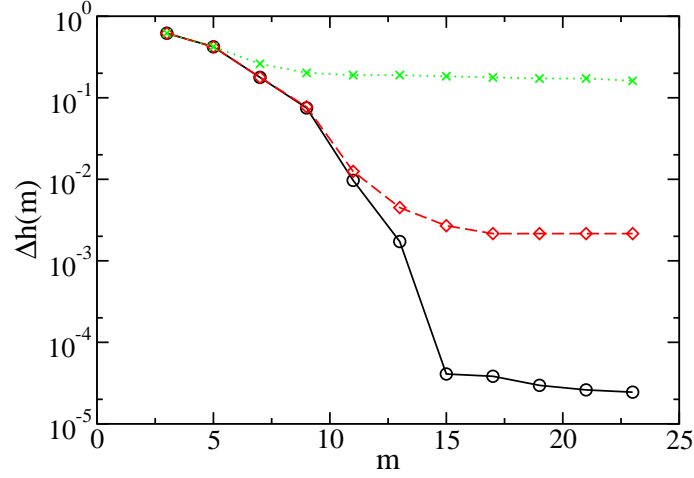


Fig. 5. Indeterminacy in the chain of Duffing oscillators (3) with $\gamma = 0.103$, $D = 0.0263$, $\omega = 0.56$, $T_1 = T_2/16$ and $T_2 = 8, 18, 20$ (from top to bottom).

values that correspond to ordered and irregular behaviour. There we see that the perturbation spreads only in the latter case (see the right panel). In the

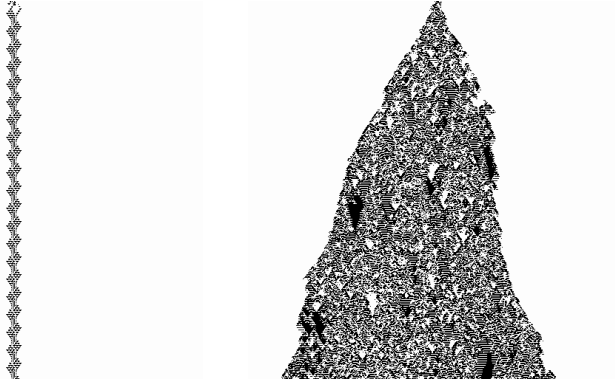


Fig. 6. Propagation of initially localized perturbations in the coupled map lattice for the same values as in Fig. 4. Time flows downwards.

CA language, the velocity v_f is often named the “Lyapunov exponent” [21]. In fact the evolution equation of an elementary CA can be formally written as a mapping of \mathcal{R}^2 into itself,

$$u^l(t+1) = F^l(u^l(t), u^r(t)) \quad u^r(t+1) = F^r(u^l(t), u^r(t)) \quad (8)$$

where $u^r(t) = \sum_{\geq 0} s_i(t)2^{-i}$, $u^l(t) = \sum_{i < 0} s_i(t)2^i$ and $s_i(t) = 0, 1$ (for the sake of simplicity we refer to binary automata). In general F^l and F^r are highly singular functions, but this does not forbid to define a sort of Lyapunov exponent from the growth rate of an arbitrarily small perturbation δ . In practice, if two configurations differ only in the interval $[-r, r]$, we can equivalently say that the representation points in \mathcal{R}^2 are separated by a distance $\delta \approx 2^{-r}$. Moreover, if the spatial region where the two configurations differ increases with a velocity v_f , we can state that the \mathcal{R}^2 distance grows as $\exp[(v_f \log 2)t]$, thus confirming that, apart from a multiplicative factor, the velocity plays the role of a Lyapunov exponent. In coupled map lattices, the local variable is continuous rather than binary, but this does not change the substance of the argument.

5 Relationship with deterministic chaos

The original model where SC has been observed for the first time has a peculiarity, namely, the discontinuity of the mapping [3]. As a result, the distance between two arbitrarily close trajectories can suddenly become of order $\mathcal{O}(1)$, when they find themselves on opposite sides of the discontinuity. It is therefore reasonable to study the continuous version of the model, i.e. to assume $\eta \neq 0$ in (2). In the limit $\eta \rightarrow 0$, the map (2) reduces to the original discontinuous system.

Already at the level of the single map (i.e. without invoking any spatial coupling), the introduction of an additional branch may drastically modify the structure of the corresponding dynamical system. This is clear in the simple case $q_1 = q_2 = 0$, $p_1 = p_2 = 2$. For $\eta = 0$, the topological entropy is $H = \ln 2$, as the map corresponds the Bernoulli shift; however, for any arbitrarily small, but finite, η -value, the appearance of a third branch induces a jump to $H = \ln 3$. For the parameter values that correspond to the SC regime discussed in the previous section, the consequence of a finite η -value is even more striking, as H is strictly equal to zero for $\eta = 0$, while it is finite for $\eta = 0^+$. This can be understood, by performing a slightly nonconventional symbolic analysis. Let us start by recalling that for the original parameter values, there exists a stable period-3 orbit, whose points are ordered as $p_1 < p_2 < x_1 < x_2 < p < 3 < 1$. Because of the third contracting branch, the interval $[x_2, 1]$ is asymptotically squeezed to a point, so that we can identify the leftmost point x_2 , with the right border of asymptotically distinct trajectories. Analogously, the interval $[0, p_1]$ is also squeezed to zero and we can accordingly interpret p_1 as the right border of the relevant interval. Finally $[p_2, x_1]$ is also squeezed to zero and can be neglected as well. As a result, the relevant dynamics is described by the mapping of $I_1 = [p_1, p_2]$ and $I_2 = [x_1, x_2]$: $f(I_1) = I_2$ and $f(I_2) = I_1 \cup I_2$. It is easy to show that the corresponding topological entropy is the golden mean $H = \log[(1 + \sqrt{5})/2]$.

Therefore, we can at least conclude that the introduction of a finite but arbitrarily small η induces topological chaos in an otherwise stable environment.

In the single map, the existence of a fractal chaotic repellor can induce long transients only for those trajectories that are carefully selected in the vicinity of the repellor itself. It is reasonable to conjecture that in spatially extended systems, the stable manifold of the repellor forces generic trajectories to follow an intricate arrangement of “channels” before landing on some periodic orbits. What are, however, the dynamical properties of the lattice, when finite η -values are assumed?

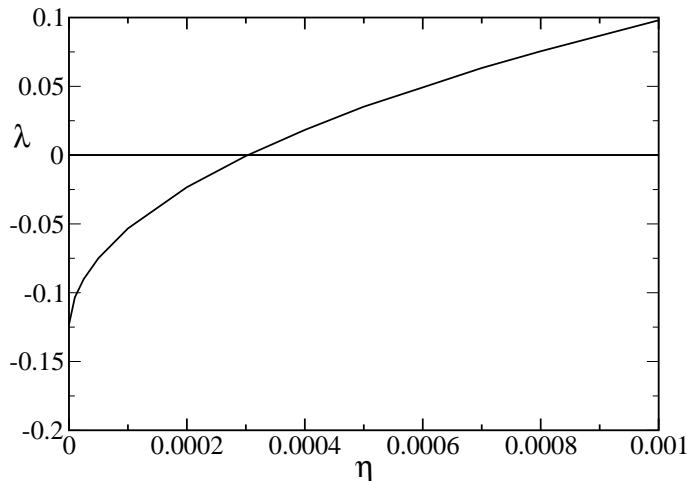


Fig. 7. Maximum Lyapunov exponent of the map lattice (2) as a function of η , while the other parameter values are the same as in Fig. 1. The results have been obtained for $N = 200$, but are practically independent of the system size.

First of all, it is important to notice that while the topological entropy jumps abruptly to a finite value, the Lyapunov exponent exhibits a smooth behaviour (see Fig. 7), i.e. for sufficiently small η -values ($\eta < \eta^* < 3 \cdot 10^{-4}$) it stays negative. This implies that the phenomenon of SC is *generic* (in the mathematical sense), even though the window of existence is (at least in this context) rather narrow. More accurate information can be extracted by performing a multifractal analysis of the Lyapunov exponent [23,24]. In particular, we have computed the probability distribution $P(\lambda, t)$ of the maximum Lyapunov exponent λ over a time span t . For sufficiently large t , the probability $P(\lambda, t)$ is expected to scale as $P(\lambda, t) = \exp[-G(\lambda)t]$ where G is a dynamical invariant whose operative definition is obtained by inverting this scaling relation, $G = -(\log P)/t$. In Fig. 8 we have plotted the results obtained for $t = 20$ and 40 . Even though the most probable and average Lyapunov exponent is negative (the spectra refer to $\eta = 10^{-4} < \eta^*$), there is

a positive tail, in agreement with the conjectured existence of a web of unstable orbits. The smoothed steps on the right of the maximum correspond to the number of times a sample trajectory is actually visiting the expanding branch. The two spectra do reasonably overlap, suggesting that the time $t = 40$ is already in the scaling regime, although finite-size corrections are still large (notice, in fact, that the maximum of G has to be, by definition, equal to 0).

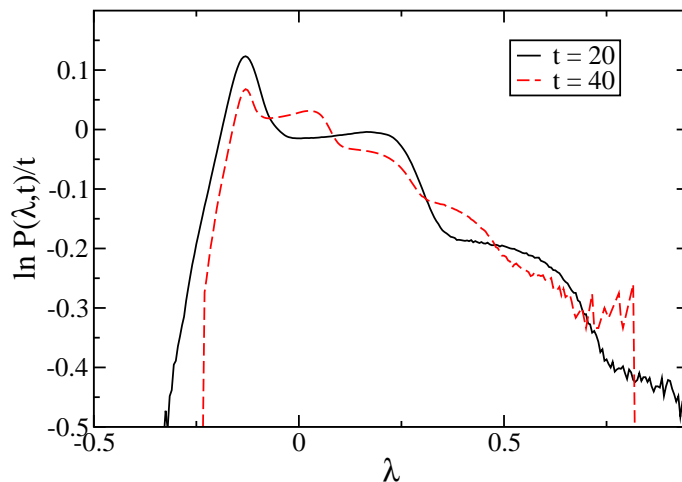


Fig. 8. Multifractal distribution of Lyapunov exponents for $\eta = 1.10^{-4}$, where the average Lyapunov exponent is still negative.

Altogether, SC appears to be somehow complementary to the blow-out phenomenon discovered in the study of synchronization transitions [25]. While analysing the stability of the synchronization manifold, it has been discovered that in some circumstances, the corresponding (multifractal) Lyapunov spectrum although mostly confined to the negative semi-axis, may exhibit a positive tail. In such a case, one has to go beyond the linear stability analysis, because whenever the distance is amplified, nonlinear terms are responsible for either bringing the trajectory back towards the manifold or letting it escape away. In the context of SC, nonlinear terms bring the trajectory back towards the “invariant manifold”, although the mechanism is perfectly efficient only in the infinite dimensional limit.

In order to clarify the mechanisms by which nonlinearities contribute to stabilizing the chaotic dynamics, it is convenient to analyse the propagation of perturbations. We start by briefly recalling the concept of convective Lyapunov exponents [26]. Given a unidimensional lattice model in the stationary regime, let us introduce a δ -like perturbation at time $t = 0$ in the origin $i = 0$ and imagine to monitor the perturbation amplitude $w_i(t)$. Kaneko and

Deissler [26] suggested that

$$w_i(t) = \exp[\Lambda(i/t)t] \quad (9)$$

where $\Lambda(v)$ represents the (exponential) growth rate of a perturbation in a frame moving with the velocity v . It is a priori obvious that for $v = 0$, one recovers the usual Lyapunov exponent, and that for large velocities one has to expect negative growth rates. In fact, $\Lambda(v)$ has a typically parabolic shape with the maximum in zero. All velocities for which $\Lambda(v) > 0$ correspond to growing perturbations. The limit velocity for linearly propagating perturbations is fixed by the marginal stability criterion $\Lambda(v_L) = 0$. Instead of determining directly $\Lambda(v)$, it is more convenient to exploit the chronotopic approach set in [27,28], and formally introduce a perturbation with a spatial amplification factor

$$w_i(t) = e^{-\mu i} u_i(t) \quad (10)$$

In our lattice model, the evolution rule for $u_i(t)$ reads

$$\begin{aligned} u_i(t+1, \mu) = & \frac{\varepsilon}{2} e^{-\mu i} f'(x_{i-1}(t)) u_{i-1}(t, \mu) + \\ & (1-\varepsilon) f'(x_i(t)) u_i(t, \mu) + \frac{\varepsilon}{2} e^{\mu i} f'(x_{i+1}(t)) u_{i+1}(t, \mu) \end{aligned} \quad (11)$$

By iterating this recursive equation with suitable boundary conditions (periodic conditions are typically optimal, as they reduce finite-size effects), we obtain the chronotopic growth rate $\lambda(\mu)$. Altogether, an infinitesimal perturbation $w_i(t) = \exp[\lambda(\mu)t - \mu i]$ with a spatial growth rate μ grows in time with an exponent $\lambda(\mu)$. The evolution of the initially localized perturbation is connected to $\lambda(\mu)$ by a Legendre transform

$$\Lambda(v) = \lambda(\mu) - \mu \lambda'(\mu) \quad ; \quad v = \lambda' \quad (12)$$

In order to determine the velocity corresponding to a given μ -value, it is necessary to compute the derivative of $\lambda(\mu)$. Since the numerical computation of derivatives is always affected by large numerical errors, it is convenient to perform a few more analytical steps [27]. By introducing,

$$u_i(t, \mu + d\mu) = u_i(t, \mu) + z_i(t, \mu) d\mu \quad (13)$$

in the recursive relation (11), we obtain an equation for the deviation $z_i(t, \mu)$,

$$\begin{aligned} z_i(t+1, \mu) = & \frac{\varepsilon}{2} e^{-\mu i} f'(x_{i-1}(t)) (z_{i-1}(t, \mu) - u_{i-1}(t, \mu)) \\ & + (1-\varepsilon) f'(x_i(t)) z_i(t, \mu) + \frac{\varepsilon}{2} e^{\mu i} f'(x_{i+1}(t)) (z_{i+1}(t, \mu) + u_{i+1}(t, \mu)). \end{aligned} \quad (14)$$

The knowledge of z_i and of u_i allows determining λ' . In fact, by taking the μ derivative in the definition of the chronotopic Lyapunov exponent,

$$\lambda(\mu) = \frac{1}{2} \lim_{t \rightarrow \infty} \frac{\|\mathbf{u}(t)\|^2}{t} \quad (15)$$

one obtains

$$\lambda'(\mu) = \lim_{t \rightarrow \infty} \frac{\mathbf{u}(t) \cdot \mathbf{z}(t)}{t \|\mathbf{u}(t)\|^2} \quad (16)$$

where \cdot stands for the scalar product. In order to better understand the selection process of the propagation velocity, it is convenient to go back to the evolution of a single exponential profile $w_i(t) = \exp[\lambda(\mu)t - \mu i]$. Its velocity is obviously $V(\mu) = \lambda/\mu$. From the Legendre transform we have that

$$\frac{dV}{d\mu} = \frac{1}{\mu} \left(\frac{d\lambda}{d\mu} - \frac{\lambda}{\mu} \right) = -\frac{\Lambda}{\mu^2}. \quad (17)$$

Since the perturbation velocity is identified by the equation $\Lambda = 0$, we see also that it corresponds to the minimum of $V(\mu_0)$. In other words, as long as the evolution is controlled by linear mechanisms, the slowest among all possible fronts is selected. Let us now turn our attention to fronts delimiting finite

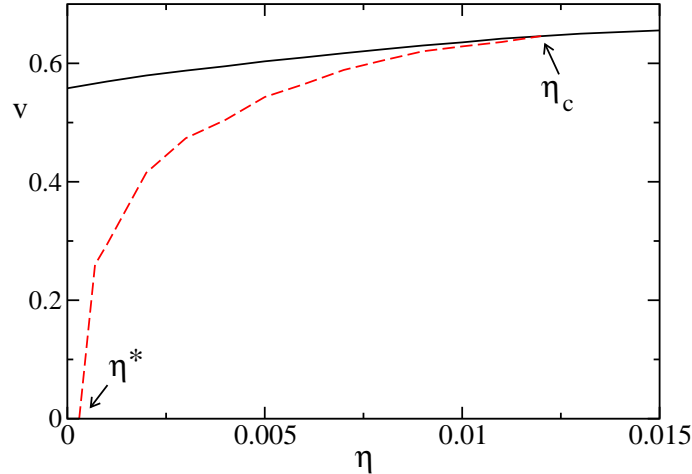


Fig. 9. Linear (v_L , solid curve) and front (v_F , dashed curve) velocity versus η . Deterministic chaos exists only for $\eta > \eta^*$. Beyond η_c , $v_L = v_F$.

perturbations. Since even such fronts must have a leading infinitesimal edge, v_F will be $v_F(\mu^*)$ for some μ^* . It is hard to imagine that μ^* is smaller than μ^0 : accordingly, either $v_F = v_L$ or $v_F > v_L$. This scenario is perfectly confirmed by the study of the model (2). Solid and dashed curves in Fig. 9 correspond to v_F and v_L , respectively. There we see that v_F is strictly larger than v_L for $\eta < \eta_c \approx 1.210^{-3}$, while above η_c the two coincide within numerical accuracy. One can also notice that the linear velocity is not defined for $\eta < \eta^*$, where the system is linearly stable and no propagation of infinitesimal perturbations can occur.

As discussed in Ref. [6], the mechanism responsible for the finite difference between v_L and v_F is that perturbations of increasing amplitude (starting from infinitesimal ones) tend to propagate faster and thereby to push the corresponding front. These results are indeed fairly general and not just restricted to the model considered in this section [29]. Moreover, this phenomenology is conceptually equivalent to that observed in the context of front propagation (see, e.g. fronts connecting steady states in reaction-diffusion systems [30,31]), that is effectively described by the famous Fisher-Kolmogorov-Petrovsky-Piskunov equation [32].

Altogether we can conclude by stating that the front velocity proves to be a useful indicator to identify the presence of SC (in spatially extended systems) from the presence of nonlinear propagation mechanisms that cannot be accounted for by linear stability analysis [6]. In such a sense, the results in Fig. 9 indicate that SC persists up to the second threshold and not just to the first one [5].

6 From order to chaos

Once ascertained that SC is a sort of extension of CA chaos to systems characterized by continuous variables, it is natural to investigate the possible phase transitions, a question that cannot even be posed in CAs, where all variables are discrete. The front propagation velocity v_F provides the right tool to assess the relative stability of the two phases. Let us, in fact, consider two initial conditions: a reference trajectory $\{x_i^0\}$, and a perturbed one $\{x_i\}$ differing only in a finite interval $-L < i < L$, where it is randomly set. If the interval where $v(i)$ is of order $\mathcal{O}(1)$ increases by eating the region where the field was initially equal to zero, we can conclude that the chaotic phase is thermodynamically stable.

In Fig. 10 we plot the results of careful computations performed with the coupled map lattice (1) for different values of the coupling strength ε . The ε -range has been selected so as to include both the ordered and the chaotic phase. In fact, we see that the front velocity is equal to zero (finite) in the left (right) part of the figure. However, these two clearly distinct phases are not separated by a point-like transition. We find instead a fuzzy region, where chaos and order alternate in a seemingly irregular manner. Is this an evidence of the complexity that is sometimes invoked to exist at the edge of chaos? Pure numerics alone is not sufficient to provide a convincing answer to such a difficult question.

An exact formulation and solution of this problem requires to control simultaneously two trajectories, a task that is nearly impossible. A simpler formulation which can nevertheless help to gain some insight on the transition consists in assuming a random evolution for the reference trajectory, and thus reducing the problem to that of characterizing the stochastic evolution of the difference field $v_i(t)$ [12]. In mathematical terms, this amounts to studying

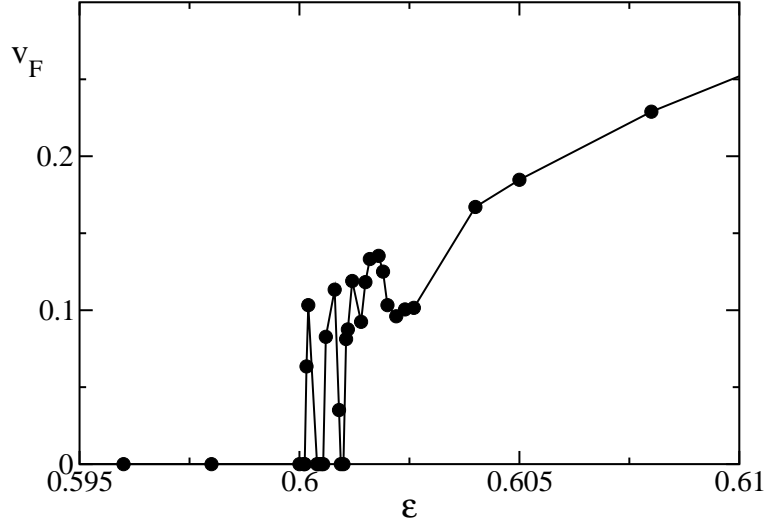


Fig. 10. Front propagation velocity in the coupled map lattice (1,2) for the same parameter values as in Fig. 1.

the equation,

$$v_i(t+1) = (1-\varepsilon)w_i(t+1) + \frac{\varepsilon}{2}[w_{i-1}(t+1) + w_{i+1}(t+1)] \quad (18)$$

where

$$w_i(t+1) = \begin{cases} v_i(t)/\eta & \text{w.p. } p = a\eta \\ av_i(t) & \text{w.p. } 1-p \end{cases} \quad \text{if } v_i(t) < \eta \quad (19)$$

$$w_i(t+1) = \begin{cases} 1 & \text{w.p. } p = av_i(t) \\ av_i(t) & \text{w.p. } 1-p \end{cases} \quad \text{if } v_i(t) \geq \eta \quad (20)$$

The stochastic $1/\eta$ amplification simulates the effect of visiting the expanding interval of the map (2). The amplification saturates to take into account the boundedness of the dynamics. This is the only element breaking the linearity of $v_i(t)$ dynamics. Moreover, for the sake of simplicity, we assume that a uniform contraction rate a (an assumption that is basically equivalent to set $p_1 = p_2 < 1$). At variance with the original deterministic model, here a detailed numerical analysis of the parameter space (a, η) , reveals that ordered and chaotic phases are separated by a standard phase transition (see Fig. 11) that belongs to the directed percolation (DP) type for small enough values of η [33] and seems to be of multiplicative noise type beyond some critical η value [34].

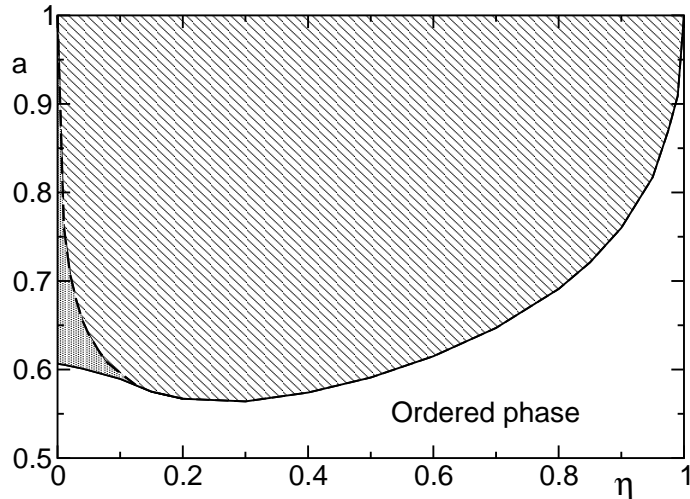


Fig. 11. Phase diagram of the stochastic model Eq. (20).

Notice that this stochastic model is even more closely related to the problem of synchronization between mutually coupled map lattices (see Refs. [35–40] for a more detailed discussion), since the assumption of a stochastic evolution is appropriate everywhere in parameter space including the critical region separating the two phases.

In the SC context, the DP transition is the most relevant one, as it occurs precisely in the regime where the evolution is characterized by a negative Lyapunov exponent. DP was introduced and is usually discussed in systems where the local variable has just two states: 0, and 1. Moreover, the dynamical rule is such that 1's cannot spontaneously appear in a sea of 0's. This is the key difference with respect to the present context, where the variable v_i is continuous and thereby the 0-state is never perfectly reached (in finite times). It is therefore necessary to introduce a threshold to decide whether the 0-state has been reached, with the related problem of having to clarify whether the results are truly independent of the threshold. In order to settle this issue, we find it convenient to determine the Finite Amplitude Lyapunov Exponent (FALE) [7]. We do so by first introducing $\tau(W)$, the average time needed by the field norm

$$\|w(t)\| = \frac{1}{L} \sum_i^L |w_i| \quad (21)$$

to become for the first time smaller than a preassigned threshold W .

The FALE can be thereby defined with reference to a sequence of exponentially spaced thresholds W_n ($W_n/W_{n-1} = r < 1$) as

$$\Lambda(W_n) = \frac{\log r}{\tau(W_{n+1} - W_n)}. \quad (22)$$

In the limit $r \rightarrow 1$

$$\Lambda(W) = \left[\frac{d\tau(W)}{d \log W} \right]^{-1}. \quad (23)$$

In the further limit $W \rightarrow 0$, $\Lambda(W)$ reduces to the usual Lyapunov exponent. In Fig. 12, we see that the FALE while being almost equal to zero at suffi-

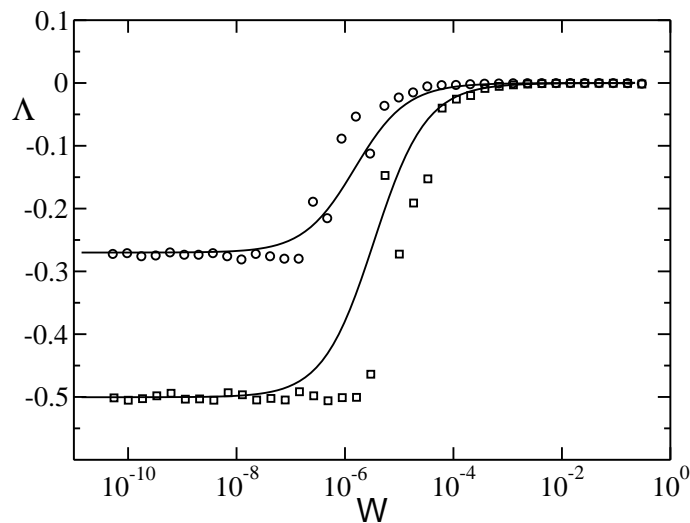


Fig. 12. Finite amplitude Lyapunov exponent of the stochastic model for two different sets of parameter values, both at criticality: circles refer to $\Delta = 0.01$, $L = 256$, $a_c = 0.6055$, squares to $\Delta = 0$, $L = 128$, and $a_c = 0.6063$.

ciently large scales, becomes equal to the true Lyapunov exponent below a certain threshold W_c . Accordingly, since for $W < W_c$, the dynamics is dominated by the usual Lyapunov exponent, we can safely conclude that when the norm becomes smaller than W_c , the absorbing state will be reached with probability one and this solves the problem of an unambiguous identification of the threshold. Moreover, detailed numerical simulations have revealed that W_c decreases faster than $1/L$, where L is the system size [33]. In discrete-variable systems, the minimal non-zero value that W can meaningfully take is $1/L$ (which corresponds to just one active site). As $W_c < 1/L$, one can conclude that in this stochastic system the scaling range is even broader than in

usual discrete systems. Now a comment about the reason why the linear stability analysis may not apply at vanishing distances. In fact, when the above defined norm of a vector is small, the field can nevertheless be sporadically of $\mathcal{O}(1)$. The behaviour of such bursts may represent an obstruction to the validity of the linear stability analysis and this is what tells Fig. 12.

Finally, we recall that FALE have been employed to characterize single maps of the type (2) revealing that for sufficiently small η and for some finite W , the FALE is indeed larger (positive) than the standard Lyapunov exponent [29]. Moreover, a generalization of the FALE to a comoving reference frame allows to formulate a marginal stability criterion that is able to predict the velocity on both cases of linear and nonlinear propagation [29]. Moreover, coupled maps (2) with $\eta = 0$ have been also analyzed by Letz & Kantz [41] who introduced an indicator similar to the FALE (i.e. able to quantify the growth rate of non infinitesimal perturbations). This indicator turns out to be negative for infinitesimal perturbations and becomes positive for finite perturbations. This means that a sufficiently large perturbation can propagate along the system due to nonlinear effects. This confirms previous observations for marginally stable systems [6].

7 More realistic models

In order to test how general *stable chaos* is, it is natural to start by asking when discontinuities or quasi-discontinuities can be expected to arise in the physical world. In fact, we have seen that the source of indeterminacy is the sudden amplification of the distance between two nearby trajectories, once they fall on opposite sides of a discontinuity. In such a case, no matter how small the initial distance is, the separation is suddenly amplified to a value of $\mathcal{O}(1)$, that is determined by the size of the discontinuity.

Before exploring the possible occurrence of such phenomena, it is important to stress that the discontinuity we are referring to is not a discontinuity in time of the type associated, e.g., to collisions. A δ -like collision induces an abrupt change of a variable (specifically, the velocity), but this affects the difference between two nearly identical trajectories only for a short (infinitesimal) time lapse, after which the trajectories come close again. This is illustrated in Fig. 13, where we have plotted the time evolution of a point-like particle bouncing elastically on the floor. In the lower panel the time evolution of the Euclidean distance is represented: only within the short time window between the collisions of the two trajectories with the floor, the relative distance becomes of order $\mathcal{O}(1)$. This is at variance with the map lattice model (1,2), where the distance, once amplified, remains large.

In the following two subsections, we illustrate some arguments supporting the idea that a natural source of such a type of discontinuities is associated with an exchange between non-commuting δ -like events.

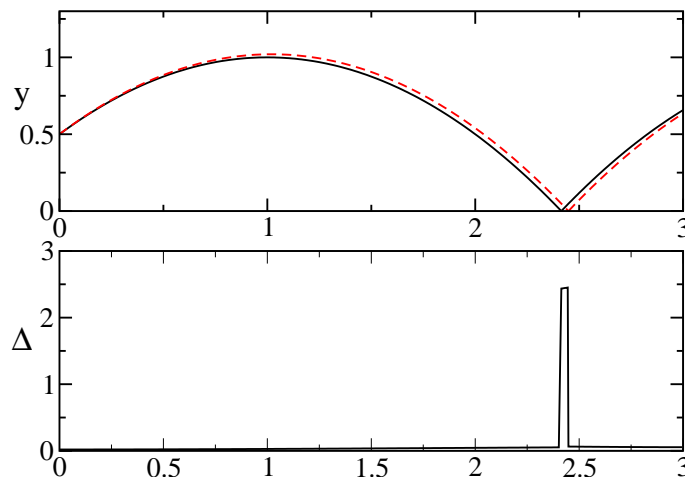


Fig. 13. Separation between two nearly equal trajectories of a point particle colliding elastically against the floor. The distance $\delta = \text{sqrt}(\delta y^2 + \delta v^2)$ is plotted versus time.

7.1 A Hamiltonian model: diatomic hard-point chain

Before introducing the model, it should be remarked that in Hamiltonian systems, conservation of volumes implies that the maximum Lyapunov exponent cannot be negative; at most, all Lyapunov exponents are exactly equal to zero. In fact, the Hamiltonian version of SC is the world of marginally stable and yet ergodic models and it often goes under the name of *pseudochaos* (see, e.g. [42]). Here, we are mostly interested in emphasizing the analogies with SC and for this reason the diatomic hard point gas (HPG) turns out to be rather appropriate also for its relationship with billiard-like models, that are often invoked in the analysis of pseudochaos.

The diatomic HPG is a unidimensional system of point-like particles with masses m and M that alternate along a line and undergo elastic collisions. In the limit $m = M$, the model is perfectly integrable, since the velocities of the two particles involved in any collision are simply interchanged. Therefore there is no mechanism leading to a diffusion in velocity space. However, as soon as the masses are assumed to be different, all numerical simulations suggest that the dynamics is ergodic. On the other hand, it is easy to convince oneself that the maximum Lyapunov exponent is still exactly equal to zero. The argument is pretty straightforward [43]: since the collision rule is linear,

$$u' = \frac{(m - M)u + 2Mv}{m + M} \quad (24)$$

$$v' = \frac{2mu - (m - M)v}{m + M} \quad (25)$$

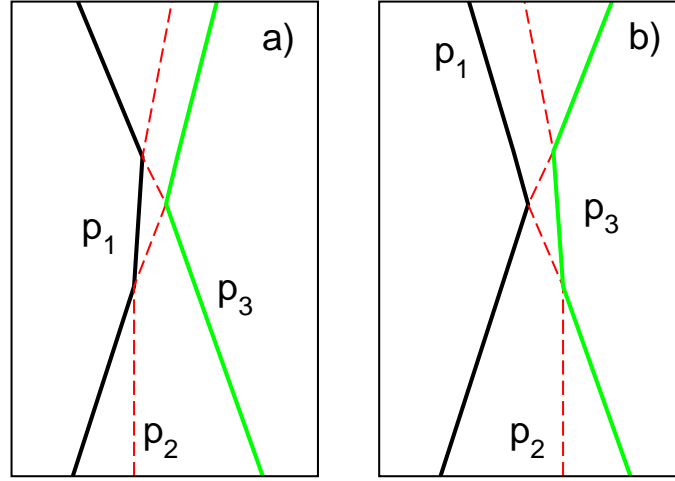


Fig. 14. Evolution of two nearly equal set of initial condition in a diatomic hard-point gas. By slightly shifting the position of the middle particle, the final velocities change abruptly when passing across the three-body collision.

both real- and tangent-space dynamics follow the same rule. As a result, the kinetic energy conservation ($\sum_i m_i v_i^2 = E$, where $m_i = m$ or M , depending on the parity of i) translates into the conservation of a suitably weighted Euclidean norm of the perturbation field, namely, $\sum_i m_i \delta v_i^2$. This means that the Euclidean norm of any vector is conserved, irrespective of its direction, so that all Lyapunov exponents are equal to zero.

In the absence of deterministic chaos, which is, therefore, the source of the stochastic-like behaviour exhibited by diatomic HPG chains? As illustrated in Fig. 14, we argue that the source are the discontinuities occurring around, e.g., three-body collisions. Let us consider an initial condition like that in the left panel of Fig. 14: it gives rise to a sequence of three collisions, 1 – 2, 2 – 3, 1 – 2 before the particles separate out. By shifting the position of the central particle (this is equivalent to moving the initial x_i variable in the CML), we pass to the condition depicted in the right panel, which gives rise to the collisions 2 – 3, 1 – 2, 2 – 3. Accordingly, the sequence of two-body collisions changes abruptly in correspondence of a three-body collision, when the three particles find themselves in the same place at the same time. As a consequence of this sudden modification, the three final velocities differ in the two cases, as it can be appreciated by comparing the two panels in Fig. 14. Only in the limit case of equal velocities, there is no discontinuity, since the final set is the same for both sequences. In the former case, when starting from the sequence v_1, v_2, v_3 , one passes first to v_2, v_1, v_3 , then to v_2, v_3, v_1 , and finally to v_3, v_2, v_1 . One can easily verify that the final state is the same in the latter case too.

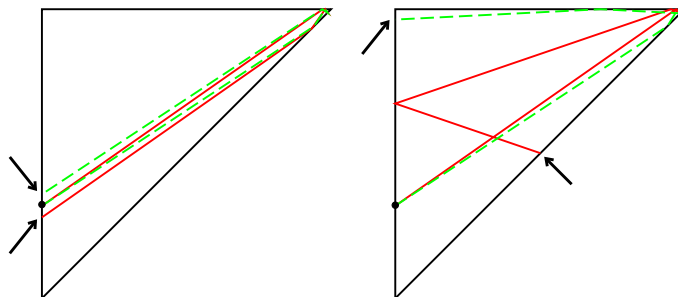


Fig. 15. Billiard-like representation of the dynamics of a chain of two particles moving in an interval with reflecting boundaries. Horizontal and vertical axes correspond to the coordinates of the first and second particle respectively. Two slightly different trajectories are plotted in each panel until the 5th collision. Left and right panels correspond to $m = M$, and $M = 2m$, respectively.

The model dynamics can be further clarified by exploring the analogy with billiard models. The connection was first discovered in Ref. [44], where the authors considered the slightly different model of hard rods. Here, we illustrate the relatively simple case of a gas of two particles P_1 and P_2 bounded to move between two fixed barriers B_l and B_r , located in $x = 0$ and $x = 1$, respectively. The linear position of the two particles can be represented as the position of a point-particle in the plane and the constraints $0 \leq x_1 \leq x_2 \leq 1$ imply that the motion is restricted to the triangular region depicted in Fig. 15. Collisions with the two mutually orthogonal triangular edges correspond to collisions with either the left or the right barrier, while those with the diagonal correspond to interparticle collisions. Finally, the three angular points correspond to the only two possible three-body collisions, $B_l P_1 P_2$, $P_1 P_2 B_r$ and to the synchronous occurrence of the two-body collisions $B_l P_1$ and $P_2 B_r$. In the equal mass case, there is a perfect correspondence between hard point gas and the triangular billiard. Accordingly, we can invoke the conjecture raised in [45] that billiards with rational angles (expressed in π units) are necessarily ergodic. The crucial difference that appears as soon as the two masses are assumed to differ from one another is that in the billiard-like representation, the mass itself assumes a vectorial character. In particular, incoming and outgoing velocities are not mutually symmetric in correspondence of a collision with the diagonal. However, the most relevant consequence is the appearance of true discontinuities. This is illustrated by comparing two nearby trajectories which undergo a different sequence of collisions. In the left panel of Fig. 15, which refers to equal masses, we see that the small difference in the initial velocity generates a slow linear increase of the mutual distance. In the right panel, which refers to $M = 2m$, the two trajectories, although starting from the same initial conditions, drastically separate out and find themselves very far apart after as few as 5 collisions (see the arrows).

7.2 Neural networks

A perhaps more interesting example of a model exhibiting stable chaos is a network of leaky-integrate-and-fire neurons, where exponentially long transients have been identified in various set-ups [46,13,47,48]. By following [13], the model dynamics for a network of N neurons can be written as a set of N differential equations

$$\dot{v}_i = c - v_i - (v_i + w) \sum_{j=1}^N \sum_m g_{ij} \delta(t - t_j^{(m)}) \quad (26)$$

where the connectivity matrix g_{ij} is defined as

$$g_{ij} = \begin{cases} G/\ell_i & \text{if } i \text{ and } j \text{ are coupled} \\ 0 & \text{otherwise,} \end{cases} \quad (27)$$

ℓ_i is the number of neurons that are connected to the i th neurons, and G is the coupling strength. Here, we will limit to consider the case of inhibitory coupling, that, in these notations, corresponds to a positive G value. All variables are dimensionless and suitably rescaled: the ‘‘action potential’’ $v_i \in [-\infty, 1]$ whenever reaches the limit value $v_j = 1$, is reset to 0 and a δ -spike is thereby emitted and received by all the connected neurons. The parameter c controls the relaxation velocity, while w quantifies indirectly the dependence of the effect of the spike on the instantaneous value of the action potential.

When all connections are active, the dynamics rapidly converges towards a stationary state characterized by a sequence of evenly spaced spikes (this is a so called splay state [49,50]). In the presence of disorder, such as, e.g., a small fraction of randomly broken links, the evolution may significantly differ, depending on the coupling strength G . Below a certain critical value, there is still a fast convergence towards an ordered state where the neurons fire in a fixed order (in agreement with Jin’s theorem [51]); for sufficiently large coupling constants, the average (over different realizations of the disorder) transient length T is exponentially large with the number of neurons [13]. This is illustrated in Fig. 16, where we have plotted the average transient for different system sizes: squares and circles correspond to $G = 0.5$ and 1.8, respectively. The solid lines are the result of a linear and an exponential fit, respectively. The exponential increase of the transient is a clear indication of SC, since at the same time, the maximum Lyapunov exponent (after removing the zero exponent corresponding to a shift along the trajectory) is definitely negative (as shown in [13]).

Which is the source of such long transients? In between the spikes, the single potentials relax independently towards c (a value that is not reached, since $c > 1$). Therefore, like in the diatomic hard point gas, the evolution is piecewise linear and one can derive an analytic expression for the map as rigorously done in Ref. [13]. In the absence of jumps between different

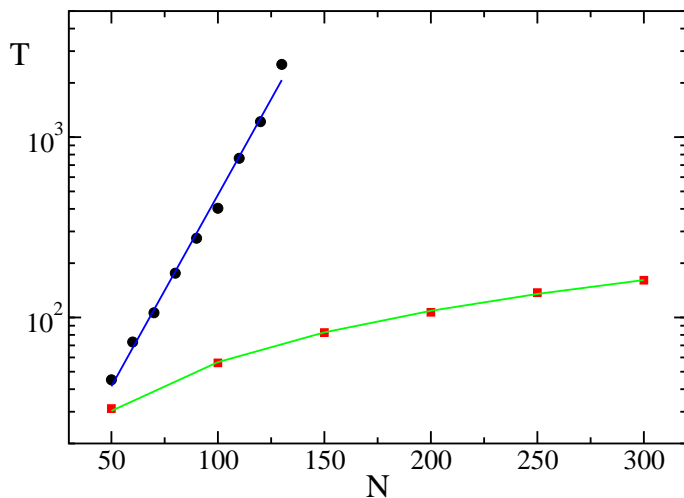


Fig. 16. Transient length for the neural network model (26) for $c = 2$, $w = 4/7$ and 5% of broken links. Squares (circles) correspond to $G = 0.5$ and ($G = 1.8$). The solid lines have been obtained by means of a linear and exponential fit, respectively.

branches, the dynamics would be globally stable; the negativity of the Lyapunov exponent is a reminiscence of such a stability. However, like in the previous cases, there are discontinuities associated with abrupt changes in the firing order of the neurons. Let us indeed consider two neurons i and j such that $g_{ji} = 0$, while $g_{ij} \neq 0$ and consider two different initial conditions: (i) $v_i(0) = v_j(0) - \varepsilon$, (ii) $v_i(0) = v_j(0) + \varepsilon$. A schematic view of the evolution is presented in Fig. 17, where the solid line corresponds to the dynamics of the i th-neuron, while dashed and dotted line denote the former and latter trajectories, respectively. There, one can see that for times larger than t_2 the two trajectories are separated by a finite distance, as a result of a discontinuity in the dynamical law. This is due to the dependence of the inhibitory effect of a spike on the actual value of v (see the multiplicative factor $(u + w)$ in Eq. (26)). Being the size of the discontinuity of the same order of the coupling strength ($\mathcal{O}(1/N)$), one might argue that this is negligible for N large enough. This is not the case, because it has to be compared with the changes induced by the smooth dynamics in between two consecutive spikes that is of the same order. Moreover, the distance between the two trajectories is even amplified to $\mathcal{O}(1)$ in the time interval $[t_1, t_2]$. As $t_2 - t_1$ is, by definition of the same order of the interspike interval, this effect too is, in principle, nonnegligible.

More recently, stable and yet irregular behaviour has been reported also in the context of a slightly different neural network, where the spike are assumed to be received with a finite delay τ and the spike effects are independent of

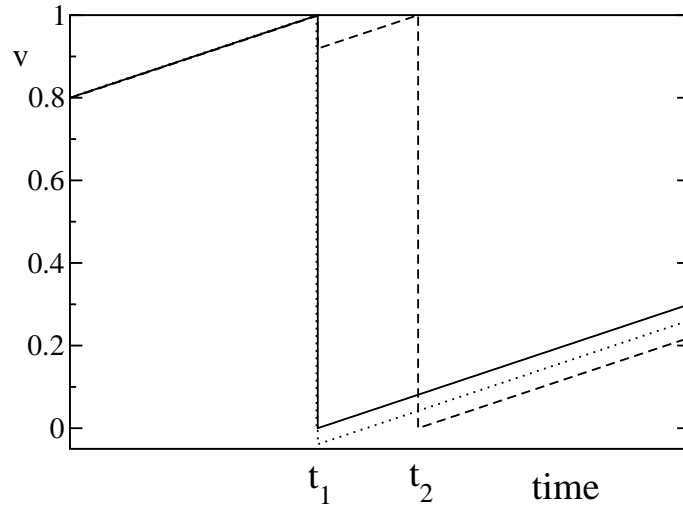


Fig. 17. Evolution of two neurons with nearly the same potential and asymmetric coupling: neuron i couples to j , but not vice versa. The dotted line corresponds to the evolution of neuron i ; solid (dashed) curve corresponds to the evolution of neuron j in case its action potential is initially smaller (larger) than that of neuron j .

v (see [47]). From the point of view of *discontinuities*, this latter property inhibits a persistent amplification of distances between nearby trajectories. Nevertheless, the finite-time amplification mechanism is still present and the very fact that long-stable transients have been observed is an indication that it lasts enough to yield “avalanches” and thereby to a self-sustained irregular behaviour. However, one should also notice that “discontinuities” are a necessary but not sufficient condition for the onset of SC.

8 Conclusions

In the present Review we have thoroughly discussed the phenomenon of *stable chaos*, a type of irregular behaviour occurring in deterministic systems that manifests itself as an exponentially (with the system size) long and stationary transient. SC differs from usual chaos in that it is characterized by negative Lyapunov exponents, but still retains some features that are reminiscent of deterministic chaos. In fact, by smoothing out the discontinuities present in the most typical SC models, induces the multifractal spectrum of the maximum Lyapunov exponent to extend to positive values. This, in turn, suggests that topological chaos (i.e. a strictly positive topological entropy) is a prerequisite for the observation of SC. However, we have shown that linear stability analysis does not provide a convincing description of relevant

properties such as the propagation of finite perturbations. In this respect, a promising indicator is represented by the finite amplitude Lyapunov exponent, although there are conceptual difficulties in extending this approach beyond the maximum exponent.

A further interesting question concerns the transition from ordered behaviour to SC. A detailed numerical analysis of a coupled-map lattice reveals the existence of a fuzzy region, where behaviour that is neither strictly ordered nor clearly chaotic has been detected. Is this just a difficulty due to strong finite size effects, or this phenomenon hides the presence of a genuinely “complex” (uncomputable) evolution? In an almost globally-coupled neural network, the transition appears to be a standard point-like phenomenon, whose universality class is however still unclear.

The most important question concerns the generality of SC. All models where SC has been observed do possess strong localized nonlinearities that may reduce to true discontinuities in phase space. The first models where SC has been observed are somehow artificial systems with no direct relationship with the physical world. However, the discussion of the diatomic hard point gas and of the network of pulse coupled neurons, has contributed to clarify that discontinuities may spontaneously emerge in models characterized by the presence of non commuting “ δ -like” events (such as two-body collisions or spike emissions). Moreover, since we have seen that SC survives a smoothing of the coupled-map model, we may also conjecture that the same holds true in these latter contexts, once we assume finite collision times or finite pulse-widths.

9 Acknowledgment

We would like to acknowledge those who have collaborated with us on this problem over the years: R. Bonaccini, F. Cecconi, M. Cencini, F. Ginelli, P. Grassberger, R. Kapral, S. Lepri, R. Livi, G.L. Oppo, and R. Zillmer. Moreover, we wish to thank M. Timme, M. Wolfrum, and S. Yanchuk for recent useful discussions. This work has been partly carried out with the support of the EU project NEST-PATH-043309.

References

1. E. N. Lorenz, *Journal of the Atmospheric Sciences*, **20**, 130 (1963).
2. J.P. Crutchfield and K. Kaneko, *Phys. Rev. Lett.* **60**, 2715 (1988).
3. A. Politi, R. Livi, G.L. Oppo and R. Kapral, *Europhys. Lett.* **22**, 571 (1993).
4. R. Bonaccini and A. Politi *Physica D* **103** 362 (1997).
5. A. Politi and A. Torcini, *Europhys. Lett.* **28**, 545 (1994).
6. A. Torcini, P. Grassberger and A. Politi, *J. Phys.* **A27**, 4533 (1995).
7. E. Aurell, G. Boffetta, A. Crisanti, G. Paladin and A. Vulpiani, *Phys. Rev. Lett.* **77**, 1262 (1996); *J. Phys.* **A30**, 1 (1997).

8. T. Tél and Y.-C. Lai, Phys. Rep. **460**, 245 (2008)
9. C. Grebogi, E. Ott, and J.A. Yorke, Phys. Rev. Lett. **50**, 935 (1983).
10. E. Ott, *Chaos in Dynamical Systems* (Cambridge University Press, Cambridge, 1993).
11. F. Cecconi, R. Livi, and A. Politi, Phys. Rev. E **57**, 2703 (1998)
12. F. Ginelli, R. Livi, and A. Politi, J. Phys. A: Mathematical and General **35**, 499 (2002).
13. R. Zillmer, R. Livi, A. Politi, and A. Torcini, Phys. Rev. E **74**, 036203 (2006).
14. I. Waller and R. Kapral, Phys. Rev. A **30**, 2047 (1984); K. Kaneko, Prog. Theor. Phys. **72**, 980 (1984).
15. L.A. Bunimovich, R. Livi, G. Martinez-Mekler, and S. Ruffo, Chaos, **2** 283 (1992).
16. P. Grassberger, *Directed Percolation: results and open problems* in "Nonlinearities in Complex Systems", S. Puri and S. Dattagupta eds. (Narosa Publishing House, New Delhi, 1997).
17. H. Hinrichsen, Adv. Phys., **49**, 815 (2000).
18. J.L. Kaplan and J.A. Yorke, Lect. Not. Math. **13**, 730 (1979).
19. P. Grassberger and I. Procaccia, Phys. Rev. Lett. **50**, 346 - 349 (1983)
20. P. Grassberger, Physica Scripta **40**, 346 (1989).
21. S. Wolfram, *Theory and applications of cellular automata* Advanced Series on Complex Systems (Singapore: World Scientific, 1986).
22. J.P. Crutchfield, Phys. Lett. A **171**, 52 (1992).
23. R. Benzi, G. Paladin, G. Parisi, and A. Vulpiani, J. Phys. A: Math. Gen. **17**, 3521 (1984).
24. G. Boffetta, M. Cencini, M. Falcioni and A. Vulpiani, Phys. Rep. **356**, 367 (2002).
25. A. Pikovsky, M. Rosenblum and J. Kurths, *Synchronization : A Universal Concept in Nonlinear Sciences*, Cambridge University, Press, Cambridge (2002).
26. R.J. Deissler and K. Kaneko, Phys. Lett. **A119**, 397 (1987).
27. A. Politi and A. Torcini, Chaos **2**, 293 (1992).
28. S. Lepri, A. Politi and A. Torcini, J. Stat. Phys., **82** (1996) 1429; J. Stat. Phys., **88** (1997) 31; Chaos, **7** (1997) 701.
29. M. Cencini and A. Torcini, Phys. Rev. E **63**, 056201 (2001)
30. W. van Saarloos, Phys. Rev. A **37**, 211 (1988); *ibidem*, **39**, 6367 (1989).
31. U. Ebert and W. van Saarloos, Physica D **146**, 1 (2000).
32. R.A. Fisher, Ann. Eugenics **7**, 355 (1937); A.N. Kolmogorov, I. Petrovsky and N. Piscounov, Bull. Univ. Moscow, Ser. Int. **A1**, 1 (1937).
33. F. Ginelli, R. Livi, A. Politi, and A. Torcini, Phys. Rev. E **67**, 046217 (2003).
34. M.A. Muñoz, in *Advances in Condensed Matter and Statistical Mechanics*, eds. E. Korutcheva *et al.* (Nova Science Publishers, New York, 2004).
35. L. Baroni, R. Livi, and A. Torcini, Phys. Rev. E, **63**, 036226 (2001).
36. V. Ahlers and A. Pikovsky, Phys. Rev. Lett **88**, 254101 (2002).
37. F. Bagnoli and F. Cecconi Phys. Lett. A **282** 9 (2001).
38. F. Ginelli, V. Ahlers, R. Livi, D. Mukamel, A.S. Pikovsky, A. Politi, and A. Torcini, Phys. Rev. E **68** 065102(R) (2003).
39. F. Bagnoli and R. Rechtman Phys. Rev. E **73** 026202 (2006).
40. M. Cencini, C.J. Tessone, and A. Torcini, Chaos **18**, 037125 (2008).
41. T. Letz and H. Kantz, Phys. Rev. E **61**, 2533 (2000).

42. P. Castiglione, M. Falcioni, A. Lesne, and A. Vulpiani, *Chaos and Coarse Graining in Statistical Mechanics*, Cambridge University Press (Cambridge, 2008).
43. P. Grassberger, W. Nadler, L. Yang, Phys. Rev. Lett. **89**, 180601 (2002); P. Grassberger, W. Nadler, L. Yang, nlin.CD/0203019.
44. S.L. Glashow and L. Mittag, J. Stat. Phys. **87** 937 (1997).
45. G. Casati and T. Prosen, Phys. Rev. Lett. **83** 4729 (1999).
46. A. Zumdieck, M. Timme, T. Geisel, and F. Wolf. Phys. Rev. Lett. **93**, 244103 (2004).
47. S. Jahnke, R.-M. Memmesheimer, and M. Timme Phys. Rev. Lett. **100**, 048102 (2008).
48. R.-M Memmesheimer, *Precise spike timing in complex neural networks* Ph.D. Thesis, Göttingen 2007.
49. S.H. Strogatz and R.E. Mirollo, Phys. Rev. E **47**, 220 (1993).
50. R. Zillmer, R. Livi, A. Politi, and A. Torcini, Phys. Rev. E **76**, 046102 (2007).
51. D. Z. Jin, Phys. Rev. Lett. **89**, 208102 (2002).